Electronic Supplementary Information

Multifunctional Pt(IV) prodrug candidates featuring the carboplatin core and deferoxamine

Sophia Harringer,[a] Michaela Hejl,[a] Éva A. Enyedy,[b] Michael A. Jakupec,[a,c] Markus Galanski,[a] Bernhard K. Keppler,[a,c] Paul J. Dyson [d] and Hristo P. Varbanov*[a,e]

[a.] Institute of Inorganic Chemistry, Faculty of Chemistry, University of Vienna, Waehringer Strasse 42, 1090 Vienna, Austria

[b.] Department of Inorganic and Analytical Chemistry, Interdisciplinary Excellence Centre, and MTA-SZTE Lendület Functional Metal Complexes Research Group, University of Szeged, Dóm tér 7, H-6720 Szeged, Hungary

[c.] Research Cluster “Translational Cancer Therapy Research”, Waehringer Strasse 42, 1090 Vienna, Austria

[d.] Institut des Sciences et Ingénierie Chimiques, Ecole Polytechnique Fédérale de Lausanne (EPFL), CH-1015 Lausanne, Switzerland

[e.] Institute of Chemistry - Inorganic Chemistry, University of Graz, Schubertstraße 1/III, 8010 Graz, Austria

Contents

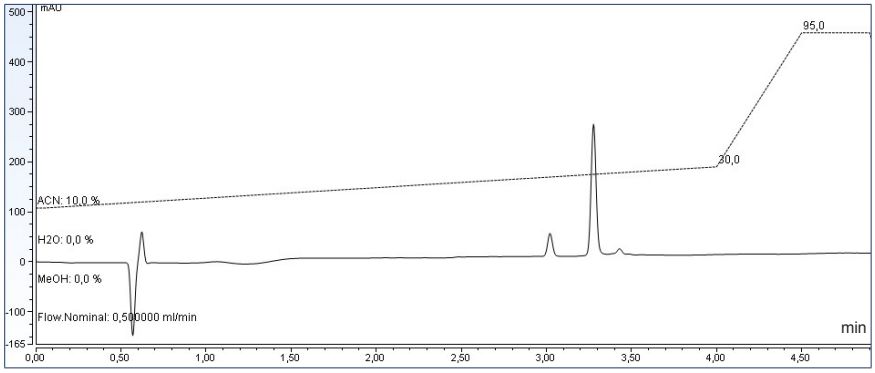

Fig. S1 HPLC purity of complex **A**: product peak at 3.28 min (~ 85%) and main impurity peak at 3.02 min (~12%). A 10-30% linear gradient of MeCN in water (with 0.1% FA) over 4 min was used; UHPLC chromatogram recorded at 225 nm is shown.

Table S1 Approximate water solubility and lipophilicity chromatographic parameters ($logk_w$ and φ_0) for the new Pt(IV)-DFO conjugates, carboplatin and DFO mesylate.

compound	aq. solub.[a]	$logk_w$	φ_0
carboplatin	9.2	-0.02	-
DFO.mes	>50	2.69	33.4
A	0.7	3.48	47.8
B	2.2	3.72	48.7
C	0.8	3.96	51.8
D	1.1	3.83	48.4
E	0.1	5.06	54.8

[a] approximate water solubility (given in mg/ml) was determined at room temperature by pipetting of minimal amounts of Milli-Q water to a weighted amount of substance until a clear solution is obtained (after shaking and sonication for 2-3 minutes)

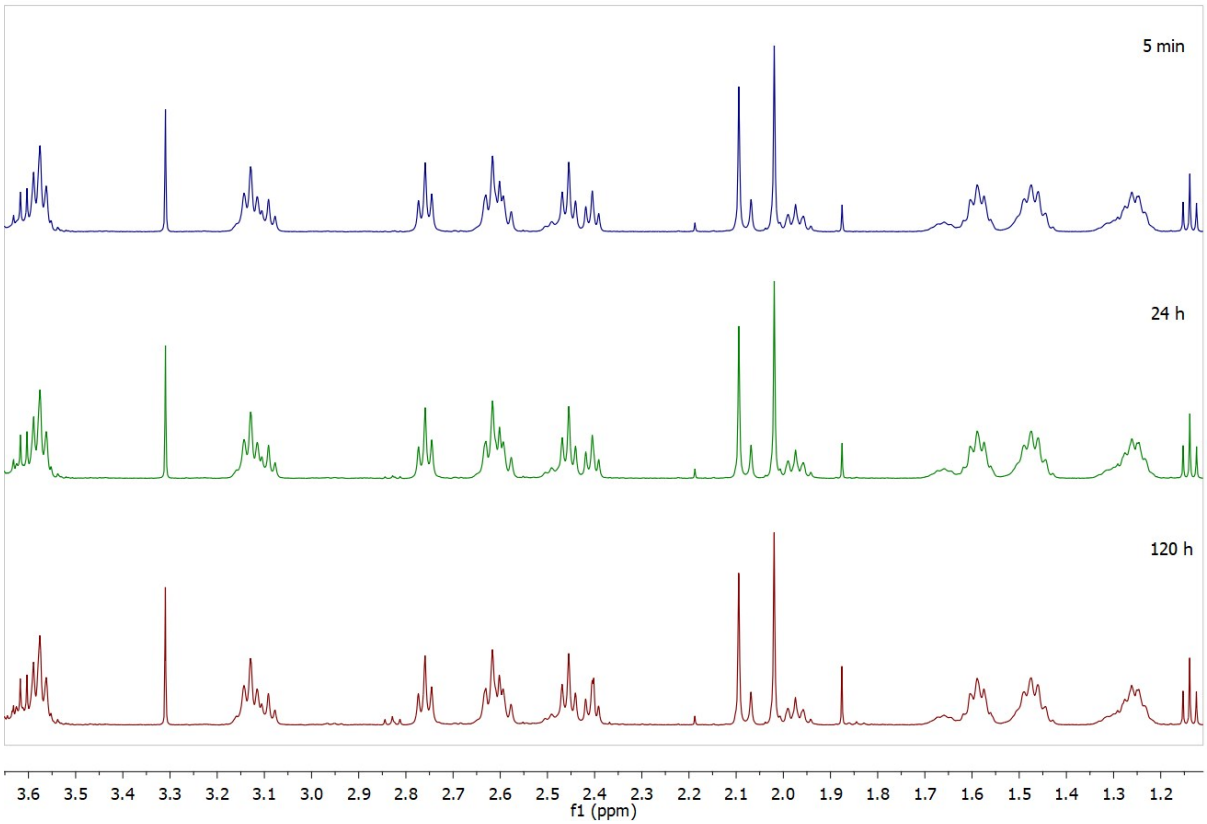

Fig. S2 ^{1}H NMR spectra of complex **B** (1 mM) in 50 mM phosphate buffer (in D_2O, pD 7.4) after addition of 25 mM ascorbic acid (top – after 5 min, middle – after 24 h, bottom after 120 h); measurements were carried out at ambient temperature.

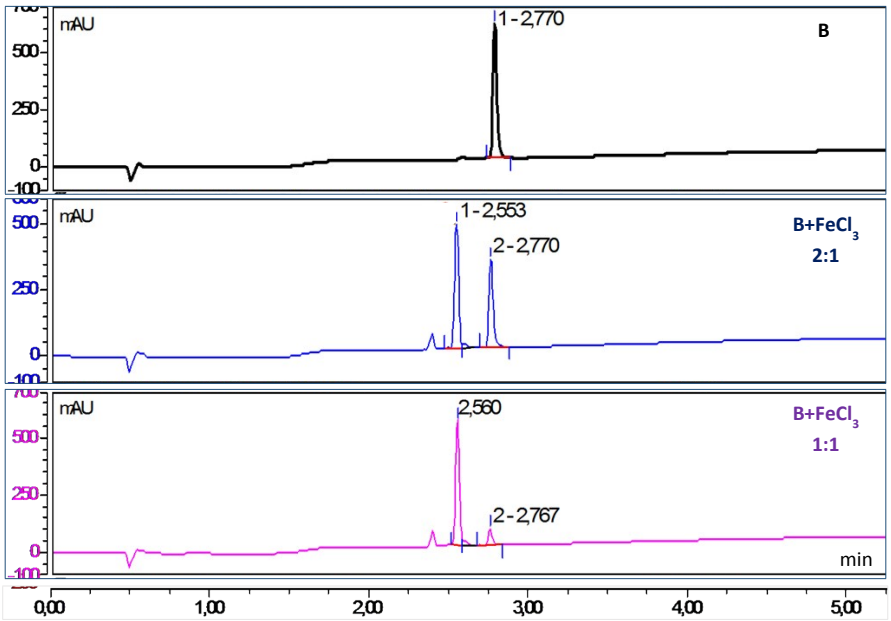

Fig. S3 UHPLC chromatograms of aqueous solution of complex **B** alone or in a mixture with $FeCl_3$ (0.5 or 1 equiv.) after 2 h of incubation at RT. A 5-85% linear gradient of MeCN in water (with 0.1% FA) was used; chromatograms recorded at 225 nm are shown.

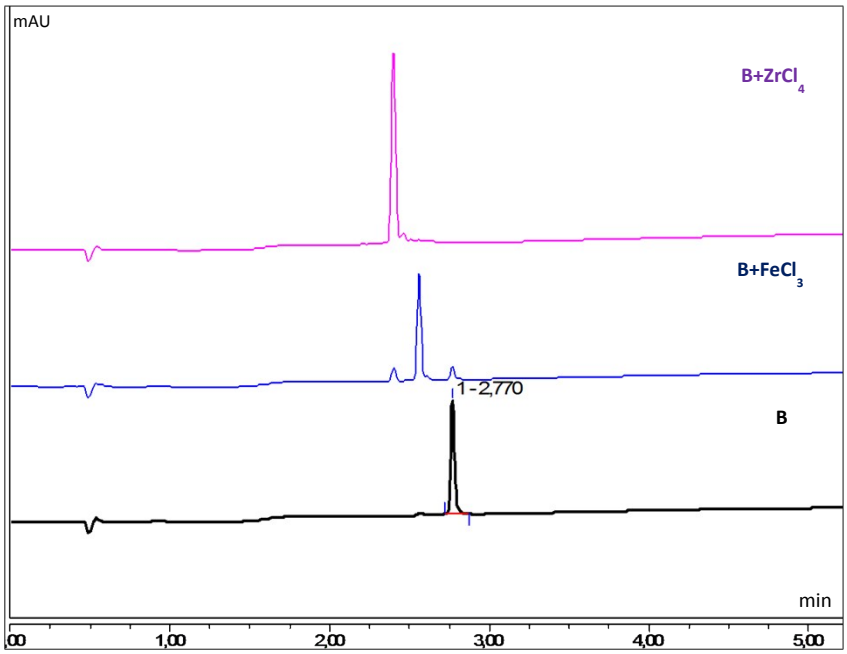

Fig. S4 UHPLC chromatograms of complex **B** alone or in a mixture with $FeCl_3$ or $ZrCl_4$ (1 equiv.) after 2 h of incubation at RT. The new species formed (t_R = 2.40 min for the Zr adduct and t_R = 2.56 min for the Fe adduct) elute earlier than parent compound **B** (t_R = 2.77 min). A 5-85% linear gradient of MeCN in water (with 0.1% FA) was used; chromatograms recorded at 225 nm are shown.

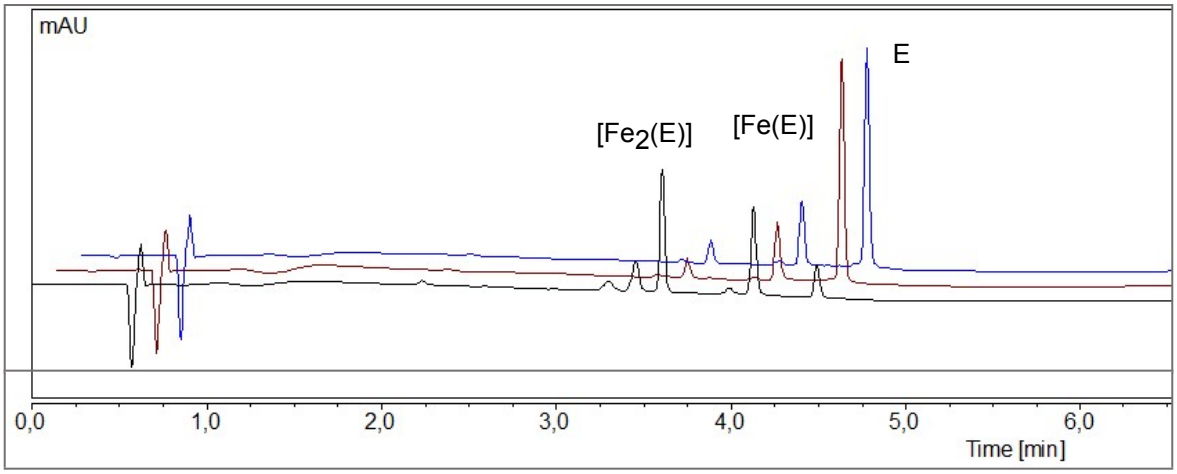

Fig. S5 UHPLC chromatograms of complex **E** incubated with $FeCl_3$ (1 equiv.) over 24 h at RT. Chromatograms show time points after 1 h, 2 h and 24 h (from back to front). Formation of new species (*i.e.*, adducts with one or two coordinated Fe^{3+}) and decrease of the peak at 4.49 min, corresponding to parent complex **E**, can be observed over time.

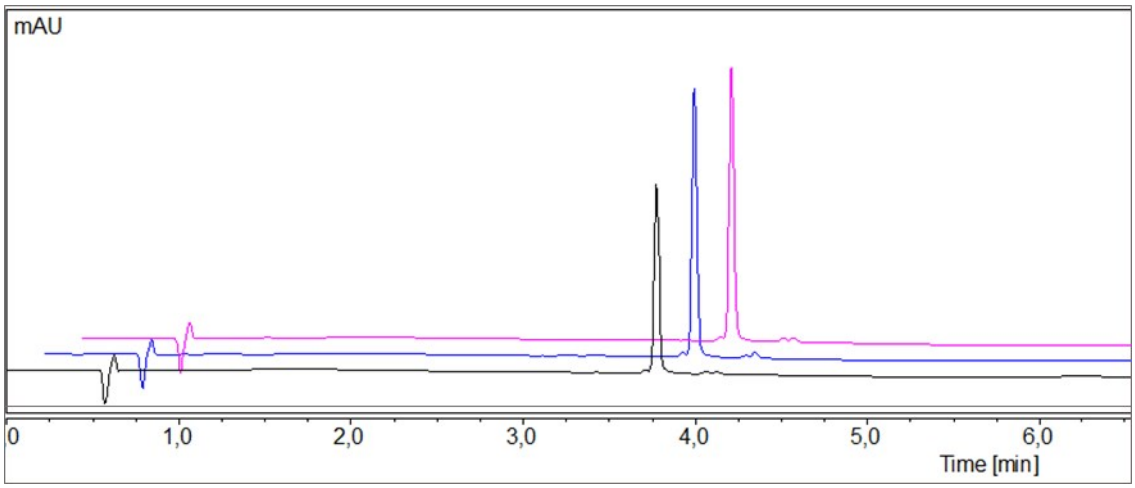

Fig. S6 UHPLC chromatograms of complex **D** incubated with $ZnCl_2$ (1 equiv.) over 24 h at RT. Chromatograms show time points after 1 h, 2 h and 24 h (from back to front). No formation of new adducts could be observed in this case. The small decrease in absorption intensity for the parent compound peak (t_R = 3.77 min) can be attributed to precipitation from solution.

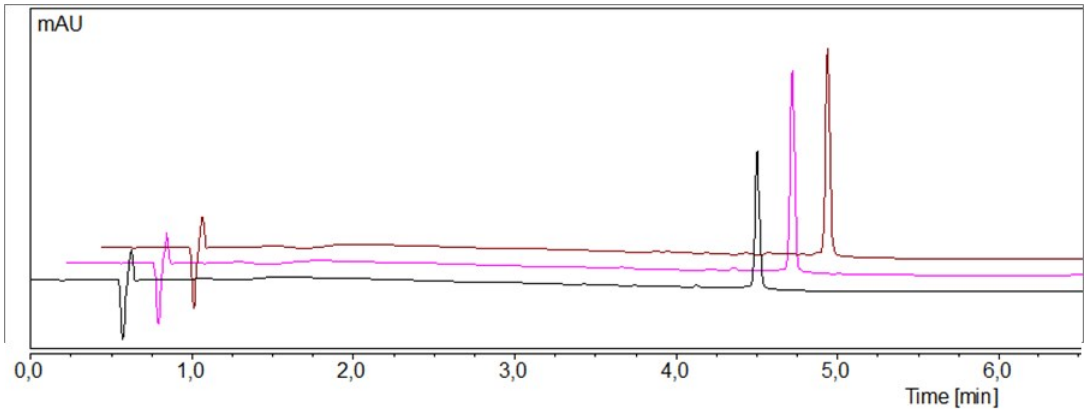

Fig. S7 UHPLC chromatograms of complex **E** incubated with $ZnCl_2$ (1 equiv.) over 24 h at RT. Chromatograms show time points after 1 h, 2 h and 24 h (from back to front). No formation of new adducts could be observed in this case. The small decrease in absorption intensity for the parent compound peak (t_R = 4.49 min) can be attributed to precipitation from solution.

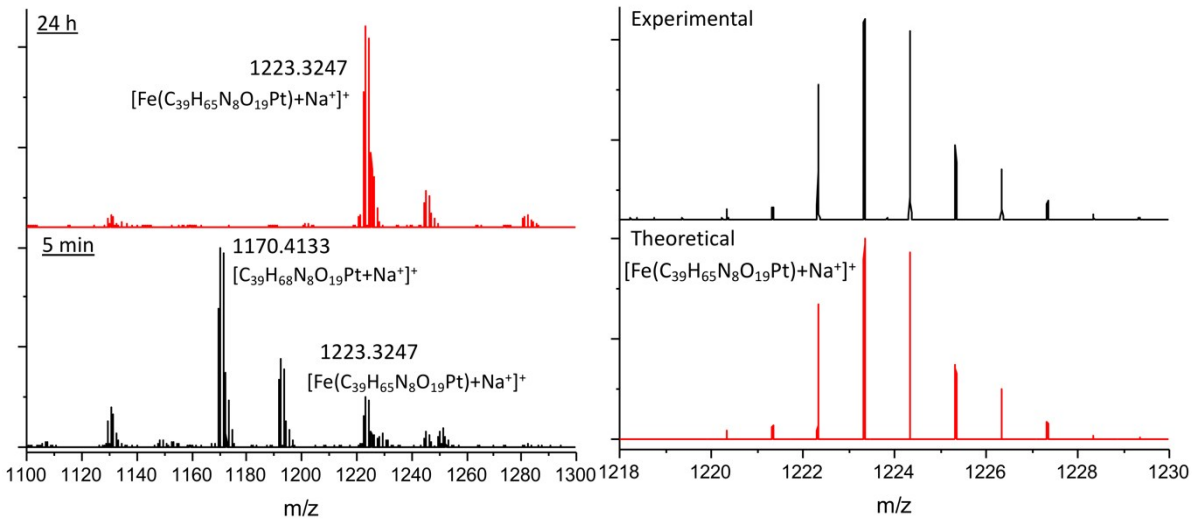

Fig. S8 ESI-HRMS (+) spectra of complex **D** incubated with $FeCl_3$ for 5 min and 24 h at RT. Experimental spectrum *vs*. simulated isotopic pattern for the Fe(III)-loaded species is shown on the right side.

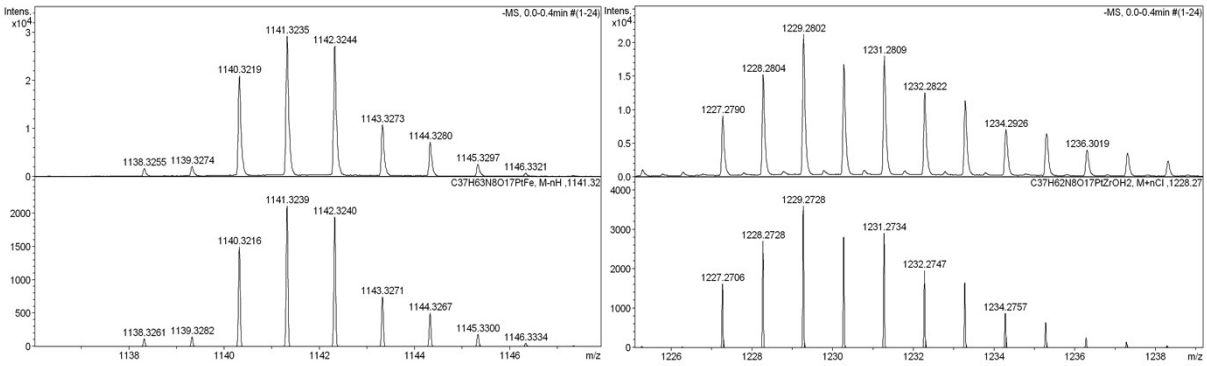

Fig. S9 Selected peaks corresponding to Fe(III) and Zr(IV) adducts found in the ESI-HRMS (-) spectra of complex **B** after 2 h of incubation with $FeCl_3$ or $ZrCl_4$, respectively. Experimental spectrum *vs*. simulated isotopic patterns for $[Fe(C_{37}H_{63}N_8O_{17}Pt)\text{-}H^+]^-$ (left) and $[Zr(C_{37}H_{63}N_8O_{17}Pt)(OH)+Cl^-]^-$ (right) are shown.

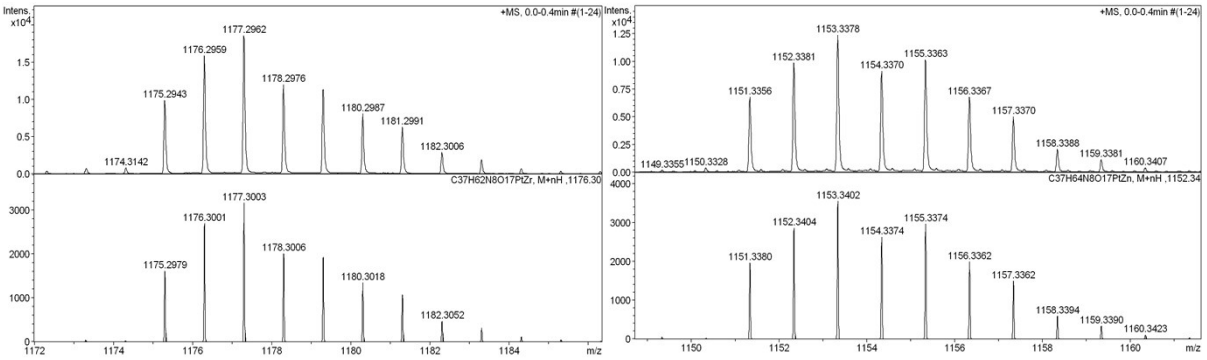

Fig. S10 Selected peaks corresponding to Zr(IV) and Zn(II) adducts of complex **B** observed in the ESI-HRMS (+) spectra of complex **B** after 2 h of incubation with $ZrCl_4$ or $ZnCl_2$, respectively. Experimental spectrum *vs.* simulated isotopic patterns for $[Zr(C_{37}H_{63}N_8O_{17}Pt)]^+$ (left) and $[Zn(C_{37}H_{64}N_8O_{17}Pt)+H^+]^+$ (right) are shown.

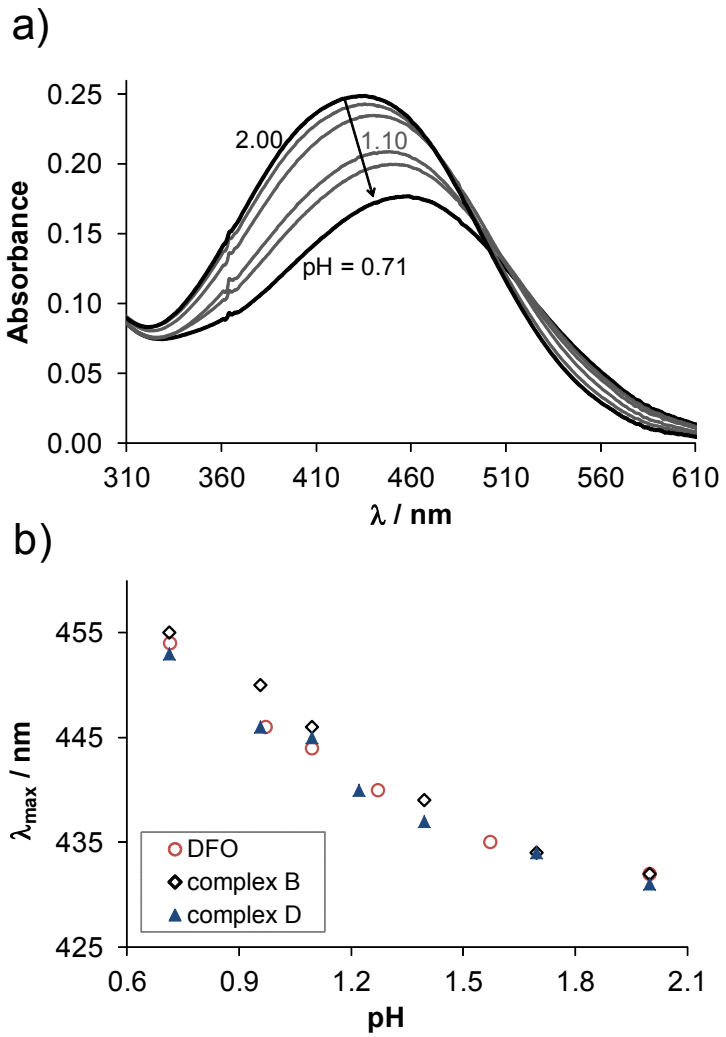

Fig. S11 a) UV-visible spectra recorded for the Fe(III) – complex **B** (1:1) system in the pH range 0.7 –2.0. b) Changes of λ_{max} values in dependence of pH in the Fe(III) – complex **B** / **D** / DFO (1:1) systems.

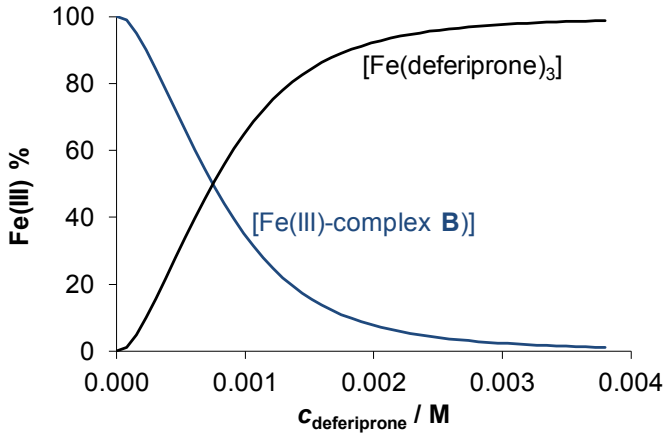

Fig. S12 Concentration distribution curves computed for the Fe(III) – complex **B** – deferiprone (1:1:x) system at pH 7.4 (x = 0 – 72.2). ($c_{Fe(III)}$ = $c_{\mathbf{B}}$ = 50 μM, $c_{deferiprone}$ = 0-3.61 mM, T = 25°C, ionic strength = 0.20 M KCl, path length = 1 cm)

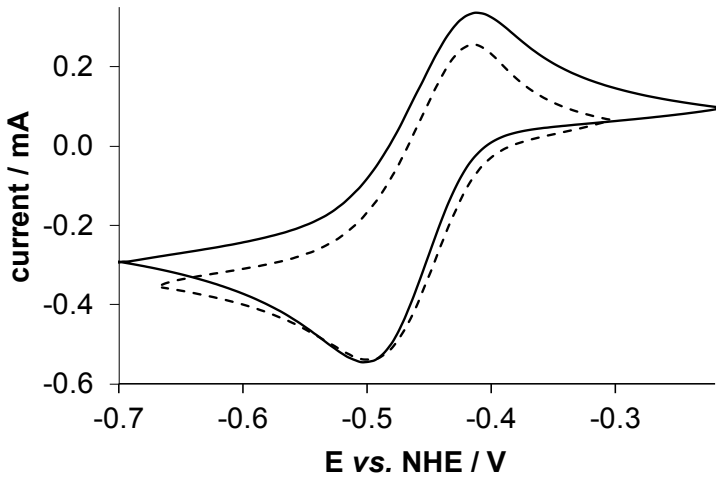

Fig. S13 Cyclic voltammograms recorded for the Fe(III) – complex **B** (solid line) and Fe(III) – complex **D** (dashed line) systems at pH 7.4. ($c_{Fe(III)}$ = $c_{\mathbf{B}\text{ or }\mathbf{D}}$ = 0.5 mM; I = 0.2 M KNO_3, T = 25°C, using Pt working and counter electrodes and Ag/AgCl/3M KCl reference electrode)

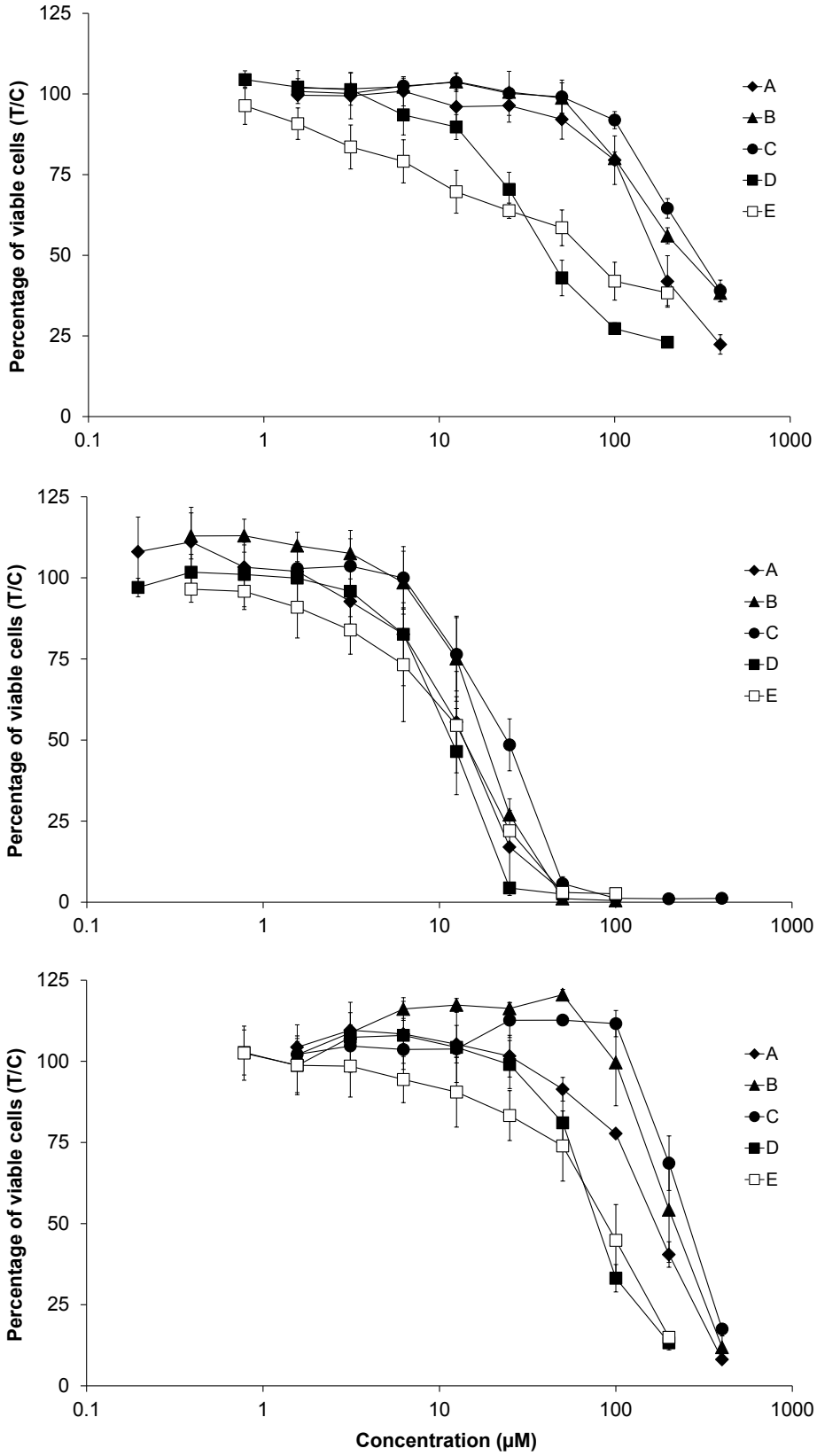

Fig. S14 Concentration-effect curves of compounds **A**–**E** in the cancer cell lines A549 (top), CH1/PA-1 (middle) and SW480 (bottom). Values are means ± standard deviations from at least three independent MTT assays (exposure time: 96 h).

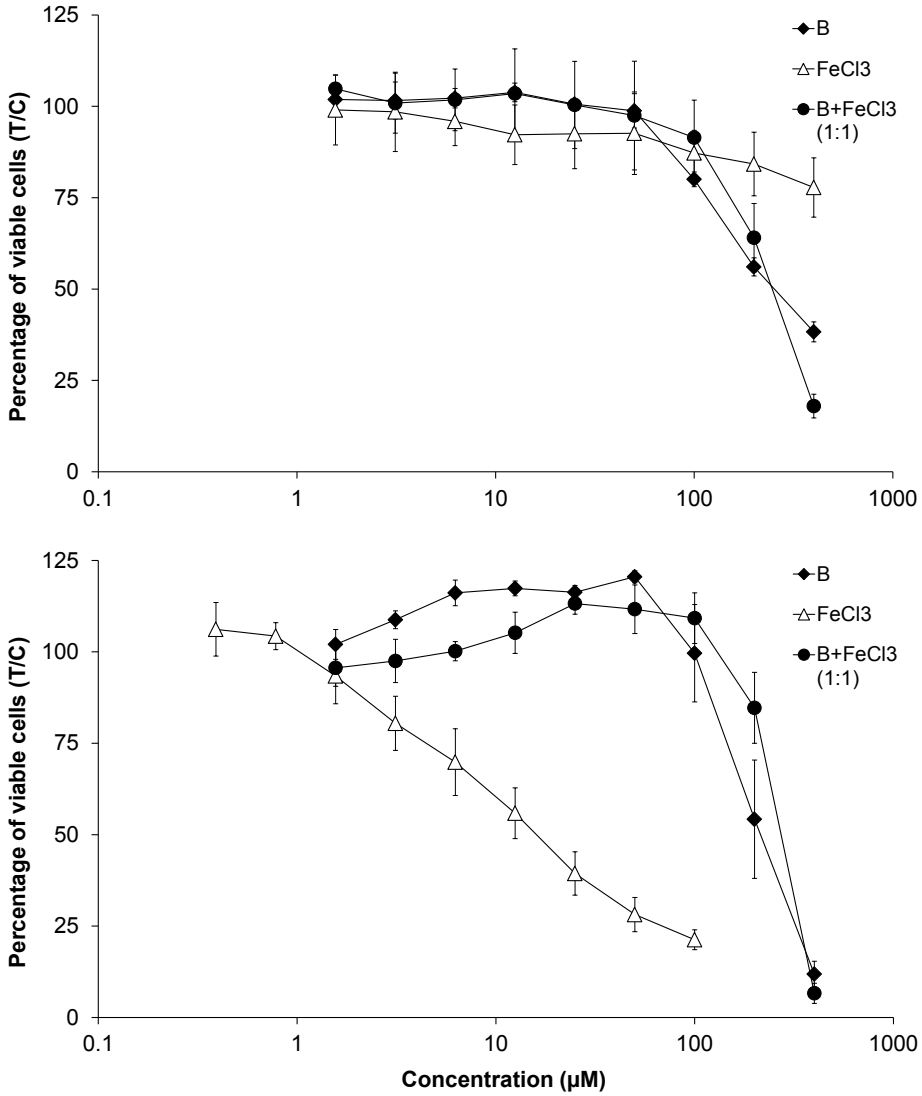

Fig. S15 Concentration-effect curves of compound **B**, $FeCl_3$ and their equimolar combination in the cancer cell lines A549 (top) and SW480 (bottom). Values are means ± standard deviations from at least three independent MTT assays (exposure time: 96 h). $FeCl_3$ on its own showed strong effect on the viability of SW480 cells (IC_{50} = 16 μM), but not A549 cells (IC_{50} > 400 μM); its cytotoxicity in SW480 cells is completely abolished upon co-incubation with complex **B**, possibly as a consequence of Fe(III) chelation. Whether the conspicuous insensitivity of A549 cells to $FeCl_3$ is connected to their expression of ABC-transporters other than P-gp or to other mechanisms remains unclear, however.

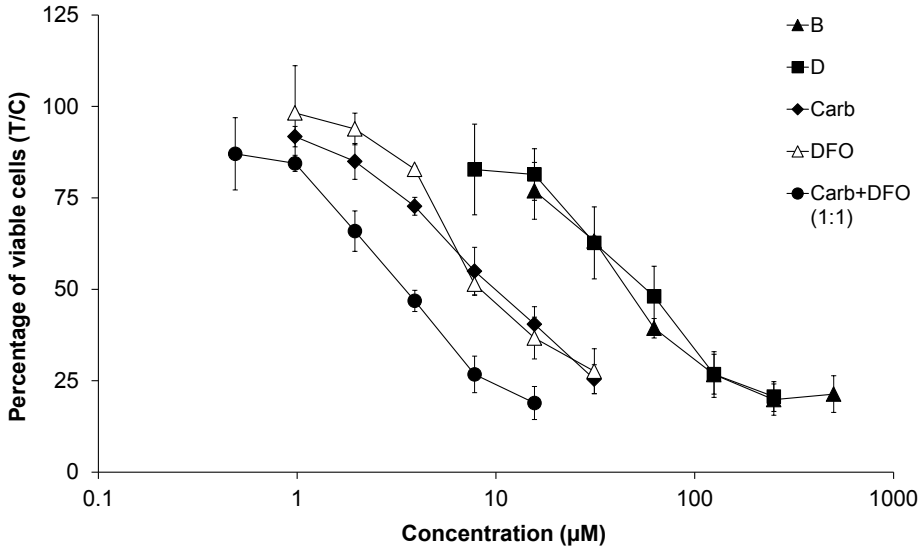

Fig. S16 Concentration-effect curves of compounds **B** and **D**, carboplatin (Carb), DFO and the equimolar combination of the latter two in multicellular tumor spheroids of the cell line CH1/PA-1. Values are means ± standard deviations from at least three independent resazurin assays (exposure time: 96 h).

Table S2. CI values for the combination between carboplatin and DFO in the investigated tumor cell models

Cell Line	Comb. ratio (carbopt : DFO)	CI values[a] at effect level of		CI_{wt} values[b]	Symbol[c]
		75%	90%		
CH1	1 : 2	0.823 (0.822 ± 0.057)	0.750 (0.750 ± 0.069)	0.766	++
	1 : 1	1.009 (1.005 ± 0.094)	0.915 (0.912 ± 0.113)	0.954	±
CH1 spheroids	1 : 1	0.713 (0.714 ± 0.078)	0.801 (0.805 ± 0.151)	0.800	++
SW480	1 : 2	1.330 (1.329 ± 0.105)	1.118 (1.202 ± 0.134)	1.220	--
	1 : 1	1.527 (1.517 ± 0.131)	1.372 (1.371 ± 0.182)	1.400	--
A549	1 : 2	0.731 (0.733 ± 0.121)	0.675 (0.679 ± 0.215)	0.704	++
	1 : 1	0.715 (0.717 ± 0.109)	0.552 (0.554 ± 0.146)	0.610	+++
	1 : 0.16[d]	0.648 (0.653 ± 0.173)	0.533 (0.546 ± 0.232)	0.559	+++

[a] CI values were calculated using CompuSyn; the values in brackets represent the means ± 95% confidence intervals, as determined from the sequential deletion analysis (S.D.A.) as a measure of the CI variability at the presented effect levels (*i.e.*, at IC_{75} and IC_{90}).

[b] Weighted average CI values, calculated as follow: $CI_{wt} = (CI_{50} + 2CI_{75} + 3CI_{90} + 4CI_{95})/10$.

[c] Degrees of synergism (+ signs) or antagonism (- signs) are based on the ranges of CI_{wt} values as described in *Pharmacol. Rev.*, 2006, **58**, 621: (±) near additive effect, (+) slight synergism, (++) moderate synergism, (+++) synergism, (++++) strong synergism; antagonism is divided in the same way, except using "-" signs.

[d] data taken from *PLoS One*, 2019, **14**, e0211268.

NMR spectra

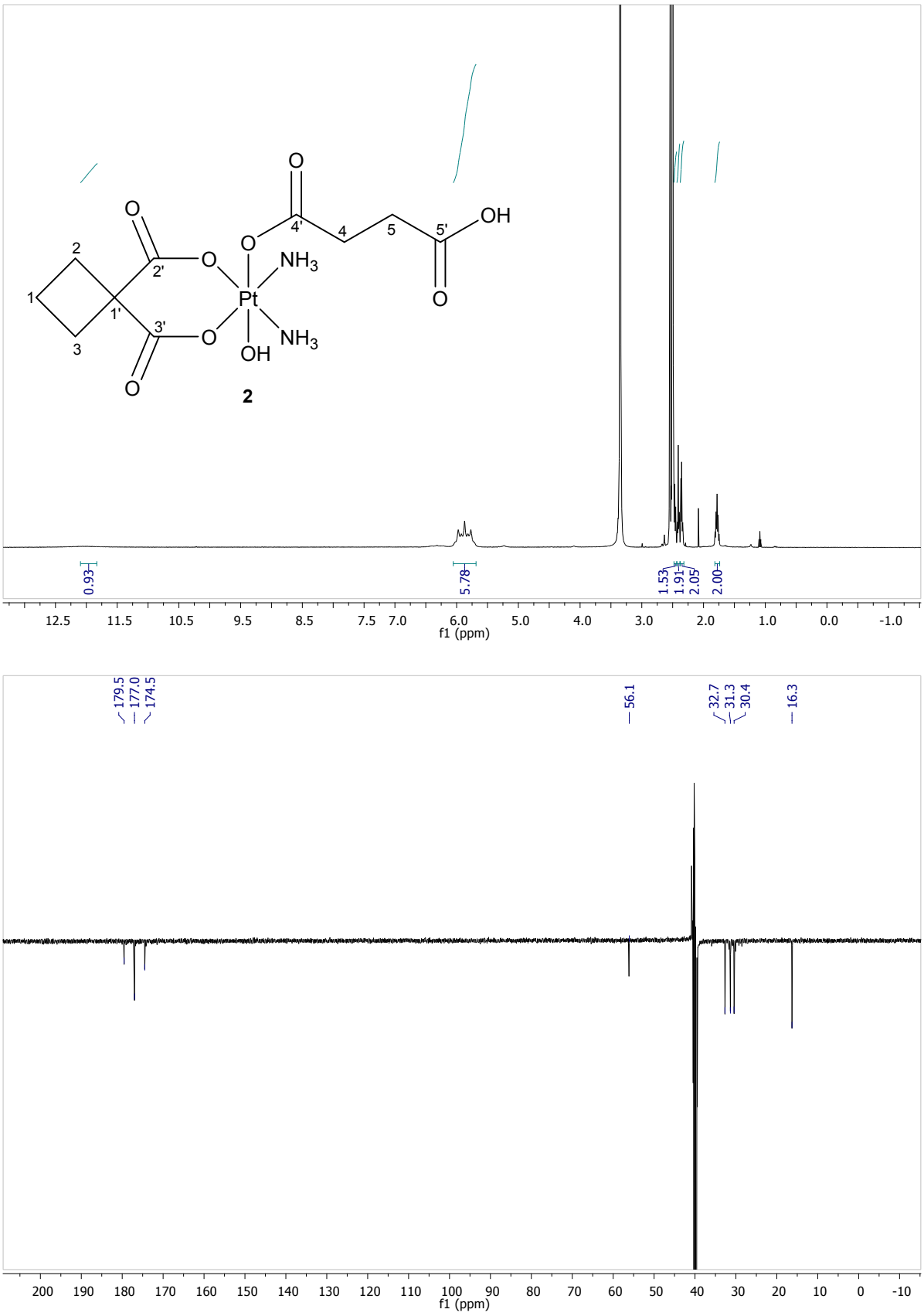

Fig. S17 ^{1}H and ^{13}C NMR spectra of precursor **2** in DMSO-d_6 at 25 °C.

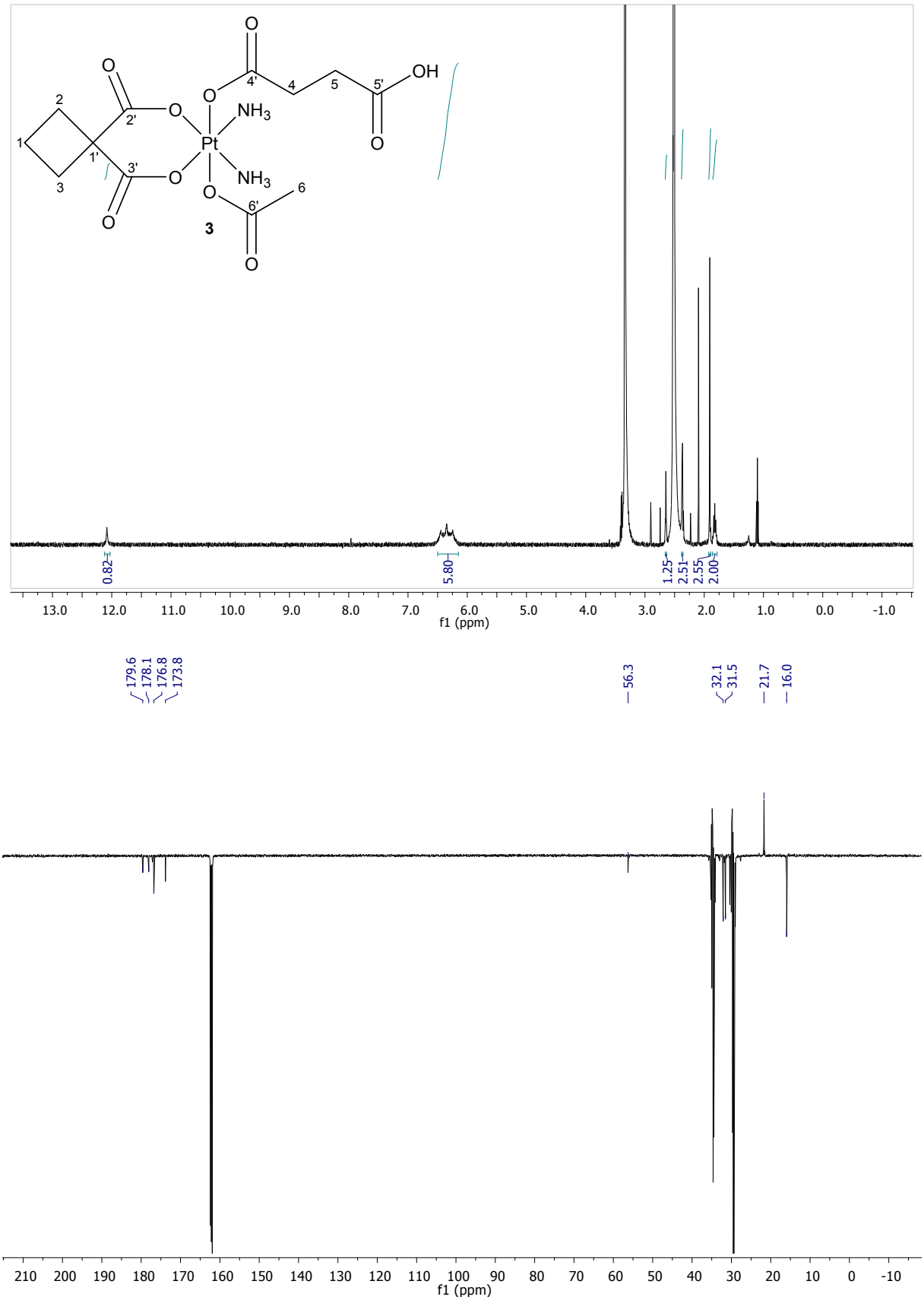

Fig. S18 ^{1}H NMR (in DMSO-d_6) and ^{13}C NMR (in DMF-d_7) spectra of precursor **3** at 25 °C.

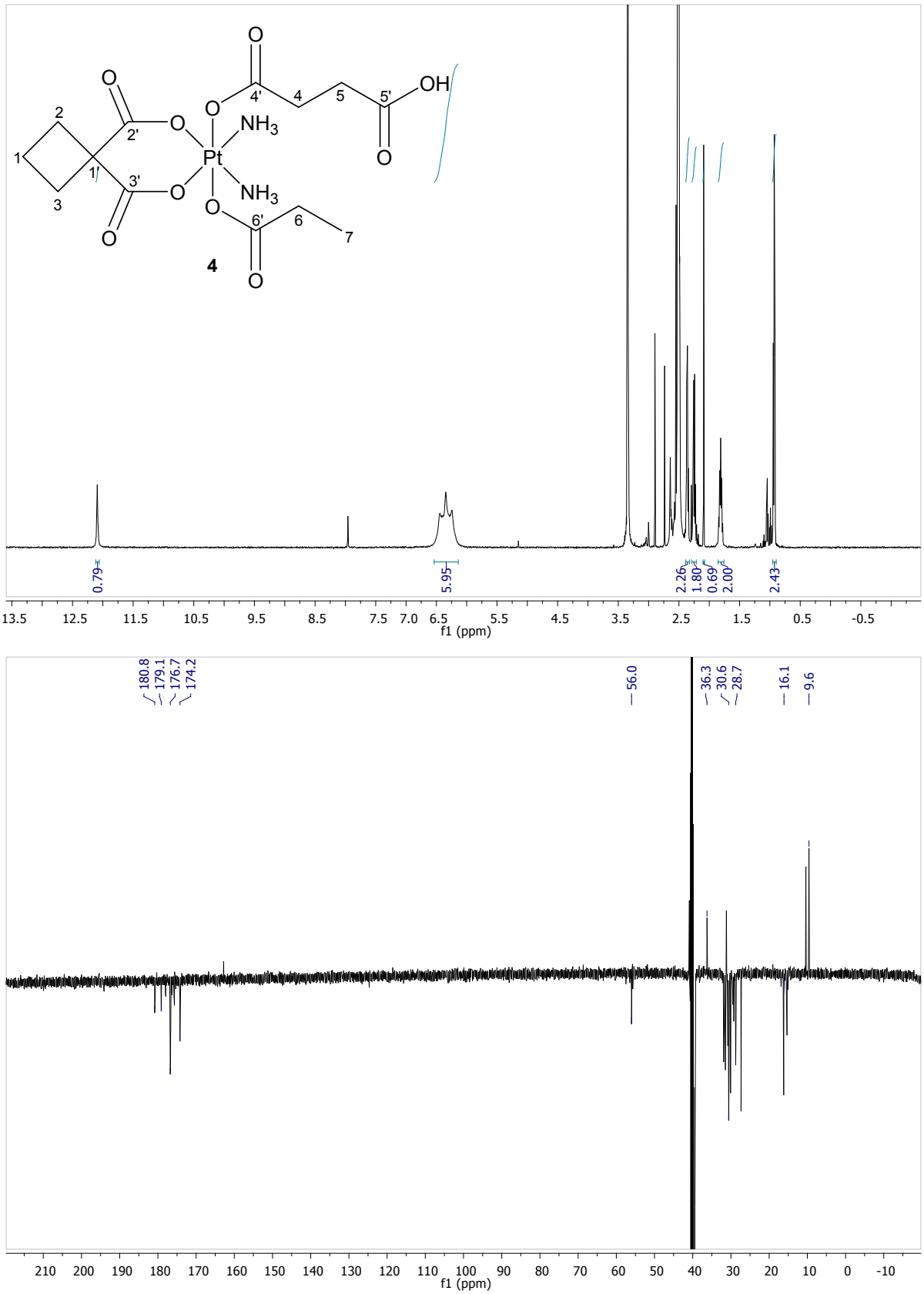

Fig. S19 ^{1}H and ^{13}C NMR spectra of precursor **4** in DMSO-d_6 at 25 °C.

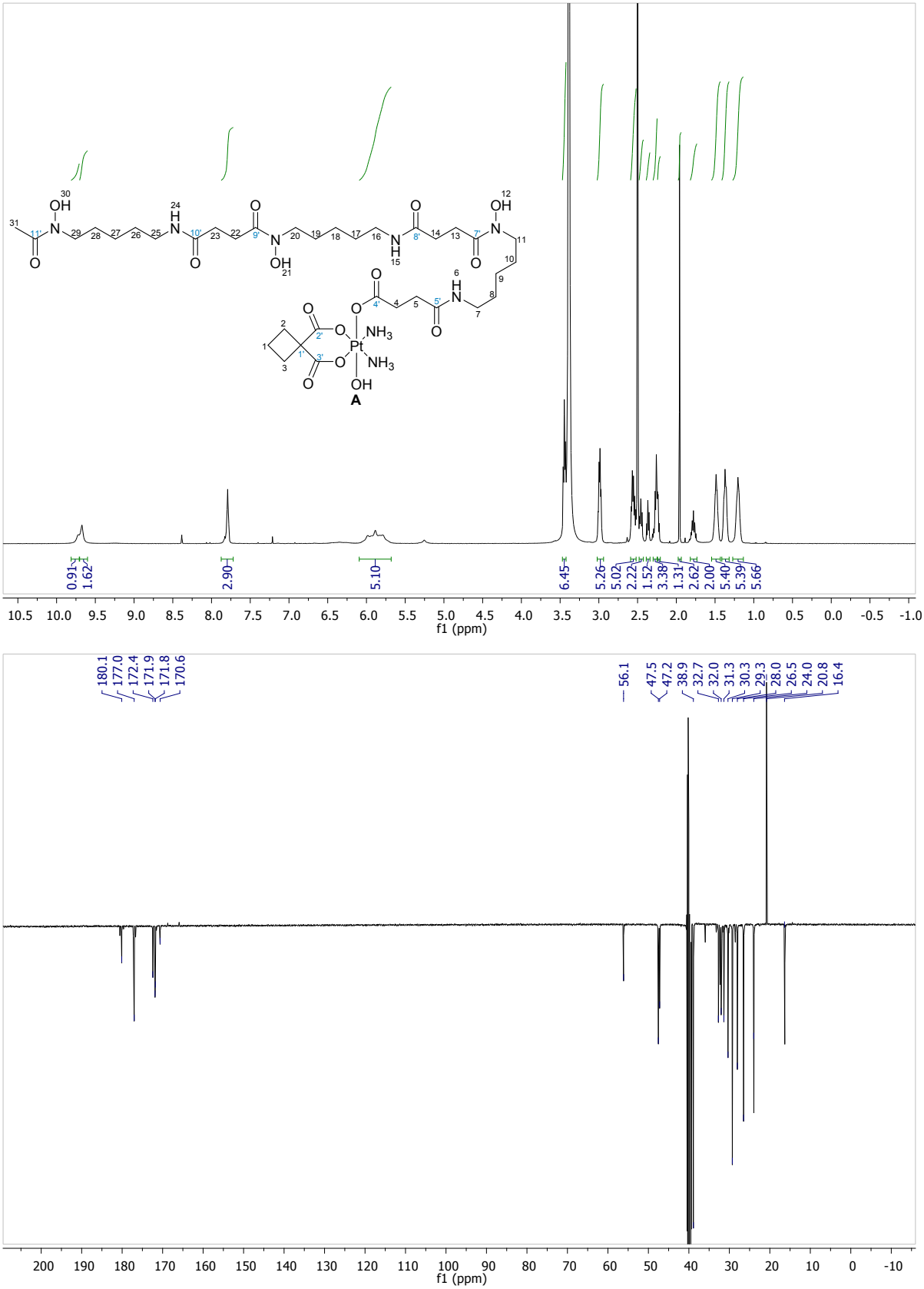

Fig. S20 ^{1}H and ^{13}C NMR spectra of complex **A** in DMSO-d_6 at 25 °C.

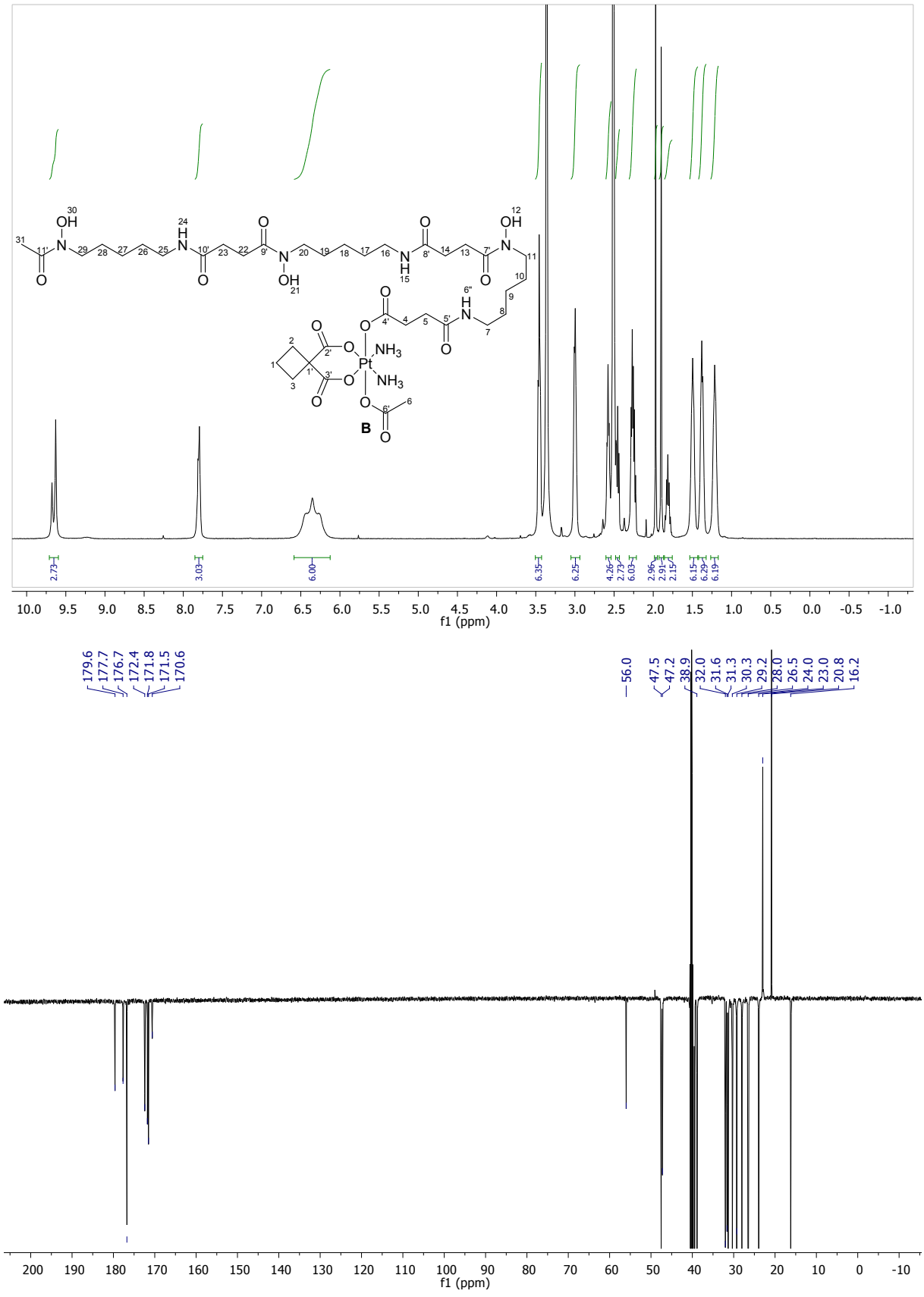

Fig. S21 ^{1}H and ^{13}C NMR spectra of complex **B** in DMSO-d_6 at 25 °C.

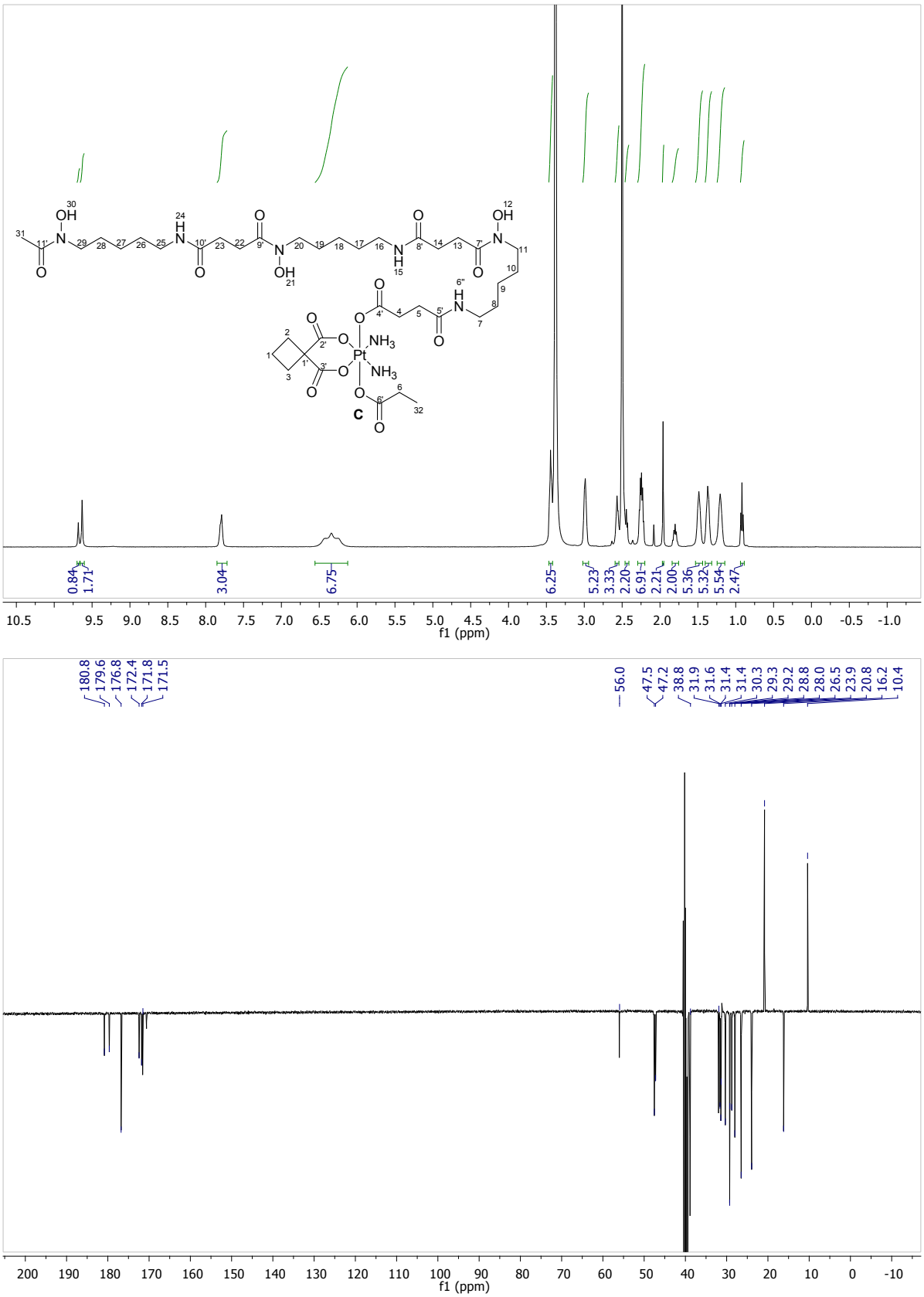

Fig. S22 ^{1}H and ^{13}C NMR spectra of complex **C** in DMSO-d_6 at 25 °C.

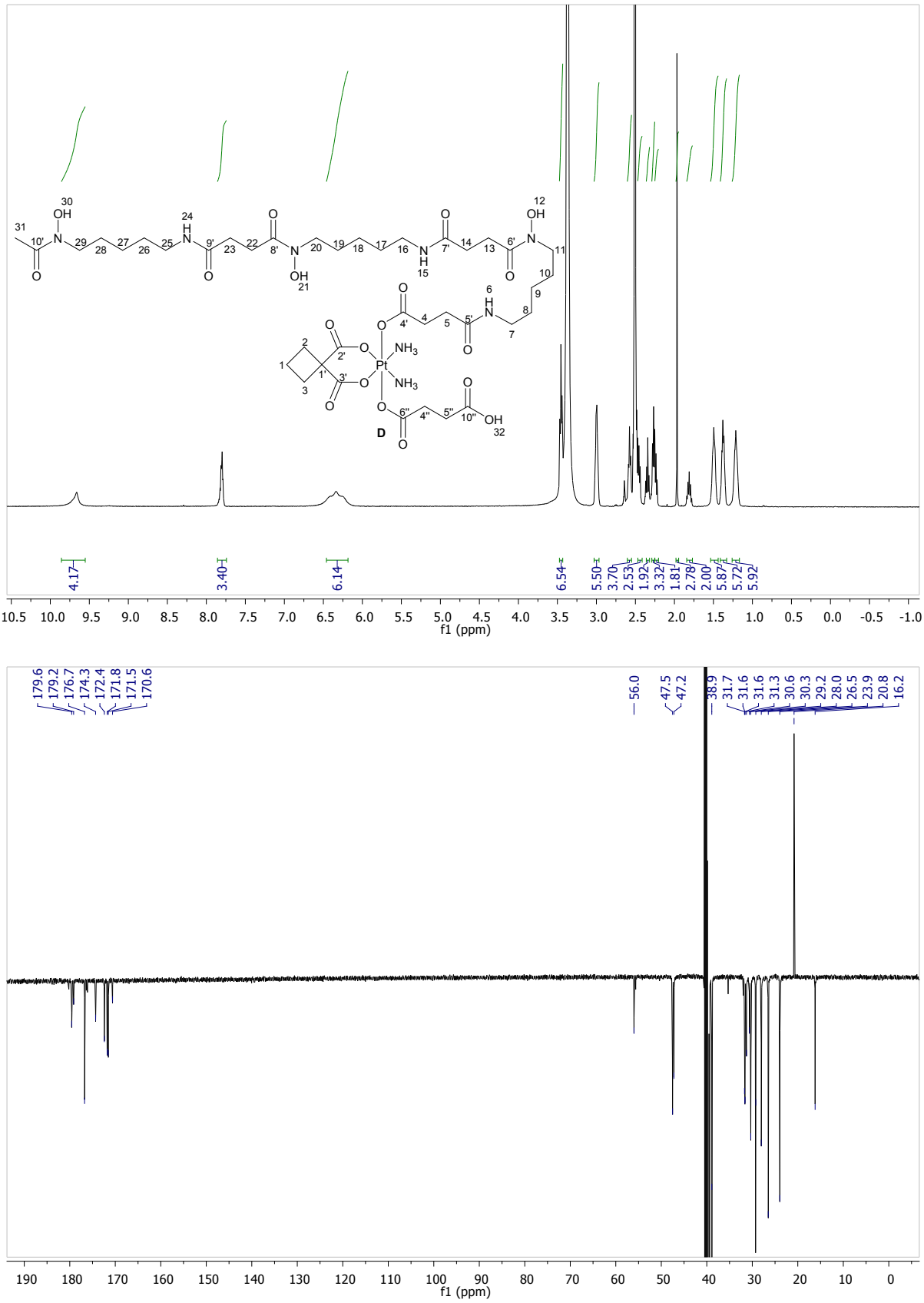

Fig. S23 ^{1}H and ^{13}C NMR spectra of complex **D** in DMSO-d_6 at 25 °C.

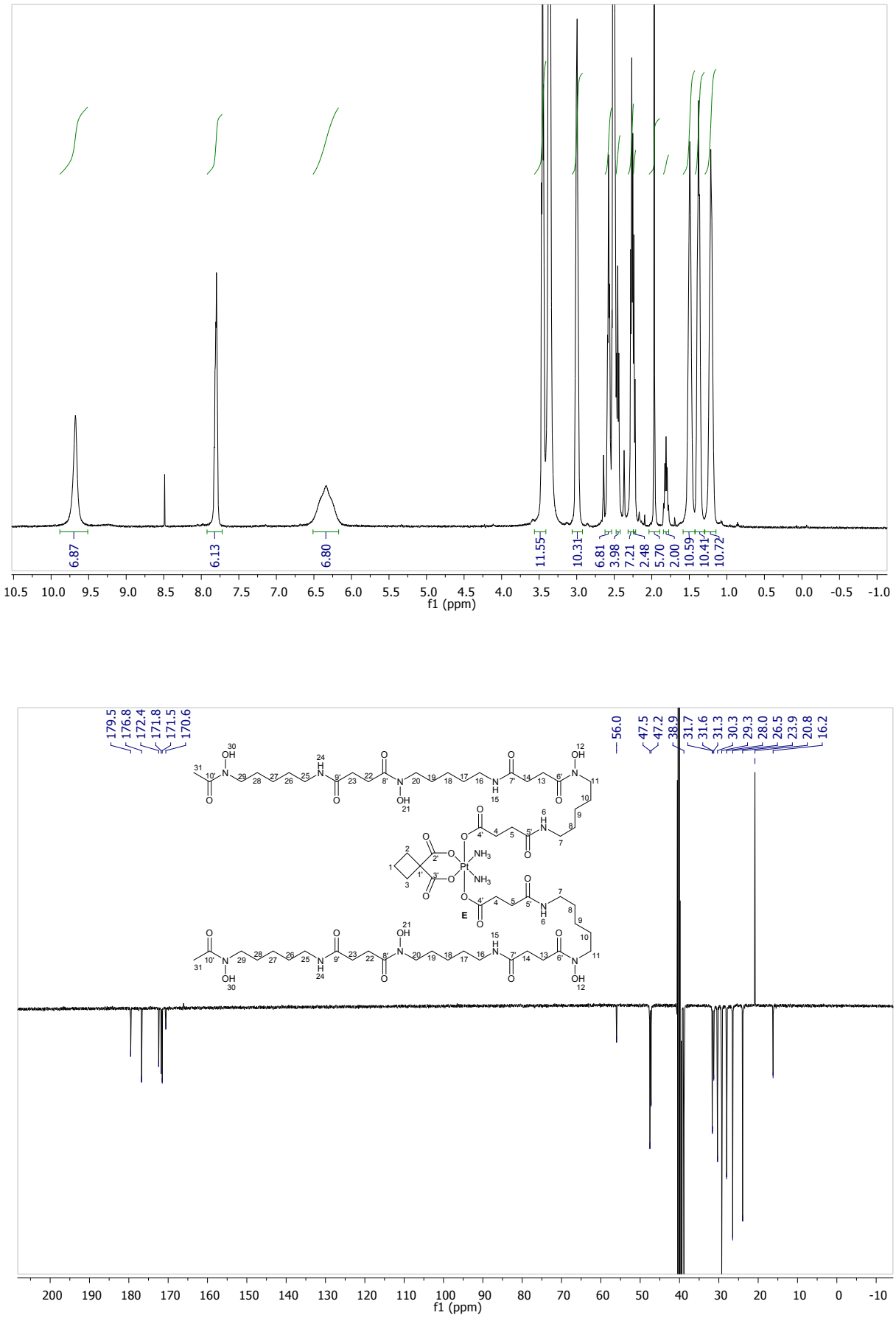

Fig. S24 ^{1}H and ^{13}C NMR spectra of complex **E** in DMSO-d_6 at 25 °C.